XL CILAMCE
IBERO-LATIN AMERICAN CONGRESS ON COMPUTATIONAL METHODS IN ENGINEERING
NOVEMBER 11-14, 2019
Praiamar Natal Hotel & Convention
Natal, RN-BRAZIL

A NUMERICAL FORMULATION FOR TWO-DIMENSIONAL ANALYSIS OF ELASTO-VISCO-PLASTIC SOLIDS AT LARGE STRAINS

Péricles R. P. Carvalho
Giovane Avancini
Humberto B. Coda
Rodolfo A. K. Sanches
periclescarvalho@usp.br
giavancini@usp.br
hbcoda@usp.br
rodolfo.sanches@usp.br
Department of Structural Engineering, São Carlos School of Engineering, University of São Paulo
Av. Trab. São Carlense, 13566-590, São Carlos, São Paulo, Brazil

Abstract. Several commonly used materials, like metals, exhibit rate-dependent plastic strains. In order to properly simulate such behavior, in this paper we present a large strain elasto-visco-plastic constitutive model and its numerical implementation. The formulation is thermodynamically based and derived from a total Lagrangian description, with the second law of thermodynamics written in the form of Clausius-Duhem inequality. In order to account for large strains, we apply the multiplicative decomposition of the deformation gradient into elastic and visco-plastic part. A neo-Hookean constitutive law is addopted for the elastic part, while for the visco-plastic part we apply a Perzyna-type model together with Norton's Law for the overstress function. Yield is defined by von Mises criterion, and a kinematic hardening of Armstrong-Frederick type is considered. The time integration of the evolution laws is performed via backward Euler method. Both plane strain and plane stress approximations are considered for two-dimensional applications, where the latter is solved numerically by a local Newton-Raphson procedure. To solve the solid mechanics problem, we employ a position based finite element formulation, which differs from traditional ones by using positions instead of displacements as nodal parameters. This approach naturally includes geometric non-linearity, being applicable to large displacements problems. Finally, we select numerical examples in order to show the characteristics of the model and its response considering different strain rates and material parameters. The obtained results show that the presented constitutive model behaves as expected and, therefore, is applicable to numerical analysis of elasto-visco-plastic materials.

Keywords: Elasto-visco-plasticity, Positional FEM, Large Strain, Perzyna Model

1 Introduction

The study of large strain plasticity has been the subject of many discussions in the field of computational solid mechanics, as it is present into several engineering problems, for instance, in manufacturing processes such as metal forming. One of the most accepted theories for the kinematic description of finite strain plastic models is the multiplicative decomposition, introduced by Kröner [1] and Lee [2] in the context of rate-independent plasticity. More developments on this subject can be seen in the works of Haupt [3] and Simo [4]. The constitutive equations can be derived from a dissipation inequality, via the principle of maximum entropy. This approach, known as thermodynamically-based, is applied, for instance, in the works of Svendsen [5], Dettmer and Reese [6] and Pascon and Coda [7].

To account for the rate-dependent behaviour of plastic strains in materials, such as metals and alloys, elasto-visco-plastic constitutive models are usually applied. In this regard, one widely employed formulations is due to Perzyna [8], who developed a model characterized by allowing a controlled non-compliance of the yield criterion, resulting in the so-called 'overstress'. For small strains, the Perzyna model is well established, being addressed, for instance, in the works of Wang et al. [9], Simo and Hughes [10] and Heeres et al. [11]. A generalization for the finite strain case was proposed by Ibrahimbegović and Chorfi [12], using a thermodynamically-based approach together with the multiplicative decomposition. Among other finite strain Perzyna models, it is worth mentioning Ponthot [13], Garino et al. [14] and Careglio et al. [15].

The elasto-visco-plastic model presented in this work is also a generalization of the classical Perzyna model, using as basis the elasto-plastic model showed in the works of Dettmer and Reese [6] and Pascon and Coda [7]. The constitutive equations are derived from the principle of maximum dissipation, where the yield criterion is imposed with a penalty-like regularization, as in the work of Ibrahimbegović and Chorfi [12], but using a Lagrangian approach instead of the originally employed Eulerian. Both isotropic and kinematic hardening laws are applied, being the latter based in the Armstrong-Frederick model presented by Vladimirov et al. [16] and Brepols et al. [17].

2 Kinematics

Let Ω_0 and Ω_1 denote, respectively, the initial (undeformed) and current (deformed) configuration of a body, and let $\boldsymbol{\zeta}$ be the configuration change function, which maps the points of Ω_0 to its corresponding coordinates in Ω_1. We denote by $\mathbf{A}$ the deformation gradient, which is the gradient of $\boldsymbol{\zeta}$ in respect to the initial configuration. Then, one can define the Green-Lagrange strain tensor by the following expression:

$$\mathbf{E} = \frac{1}{2}(\mathbf{A}^T\mathbf{A} - \mathbf{I}). \tag{1}$$

For elasto-plastic materials, Kröner [1] and Lee [2] introduced the concept of intermediate configuration, Ω_p, which represents the solid configuration when the body is unloaded to a stress-free state, such that it only contains plastic deformations. For the visco-plastic case, it can be generalized to a configuration Ω_{vp}, containing only the visco-plastic deformations. Then, we denote by $\mathbf{A}_{vp}$ the gradient of the function $\boldsymbol{\zeta}_{vp}$, mapping from Ω_0 to Ω_{vp}, and by $\mathbf{A}_e$ the gradient of the function $\boldsymbol{\zeta}_e$, mapping from Ω_{vp} to Ω_1 (see Fig. 1). Notice that $\mathbf{A}_e$ and $\mathbf{A}_{vp}$ represents respectively the elastic and visco-plastic parts of the deformation gradient. Therefore, we can write

$$\mathbf{A} = \mathbf{A}_e\mathbf{A}_{vp}, \tag{2}$$

which is known as Kröner-Lee decomposition. Analogously to Eq. (1), the elastic and visco-plastic Green-Lagrange strain tensor can be defined as

$$\mathbf{E}_e = \frac{1}{2}\left(\mathbf{A}_e^T\mathbf{A}_e - \mathbf{I}\right) \qquad \text{and} \qquad \mathbf{E}_{vp} = \frac{1}{2}\left(\mathbf{A}_{vp}^T\mathbf{A}_{vp} - \mathbf{I}\right). \tag{3}$$

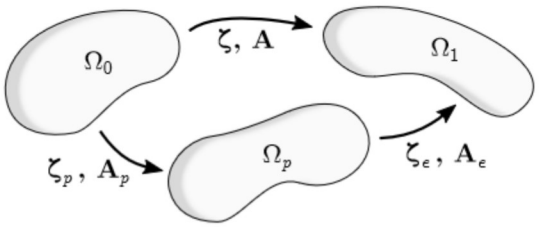

Figure 1. Initial, deformed and intermediate configurations

The volumetric strain, also known as jacobian, is given by

$$J = \det(\mathbf{A}) = J_e J_{vp}, \tag{4}$$

where $J_e = \det(\mathbf{A}_e)$ and $J_{vp} = \det(\mathbf{A}_{vp})$ are, respectively, the elastic and visco-plastic jacobian.

Furthermore, based on the rheological model presented by Lion [18], we decompose the visco-plastic deformation gradient in two parts, called, respectively, visco-plastic "elastic" and visco-plastic "inelastic" deformations: the first, denoted by $\mathbf{A}_{vp}^e$, is due to dislocation-induced lattice deformations; the second, denoted by $\mathbf{A}_{vp}^i$, represents the inelastic deformations due to slips on the crystallographic systems. By applying again the multiplicative decomposition, we write:

$$\mathbf{A}_{vp} = \mathbf{A}_{vp}^e\mathbf{A}_{vp}^i. \tag{5}$$

Then we can define, analogously to Eq. (3), the visco-plastic "elastic" and the visco-plastic "inelastic" Green-Lagrange tensors as

$$\mathbf{E}_{vp}^e = \frac{1}{2}\left[(\mathbf{A}_{vp}^e)^T\mathbf{A}_{vp}^e - \mathbf{I}\right] \qquad \text{and} \qquad \mathbf{E}_{vp}^i = \frac{1}{2}\left[(\mathbf{A}_{vp}^i)^T\mathbf{A}_{vp}^i - \mathbf{I}\right]. \tag{6}$$

3 Positional finite element method

Most of finite element approaches for solid mechanics analysis uses displacements as nodal parameters. In this work we adopt the positional finite element method, which uses current positions as nodal parameters, under a total Lagrangian description. Although for 2D solid elements the resulting positional formulation has the same features as the displacement based formulation, its derivation is didactically easier and more compact to write. Since the positional FEM is not the scope of this work, only a brief description is given in this text. For more detais, the reader should refer to the works of Coda and Greco [19], Coda [20], Coda and Paccola [21] and Coda and Paccola [22].

For each finite element domain, the initial and current positions, denoted by $\mathbf{x}$ and $\mathbf{y}$, respectively, can be written as

$$\mathbf{x}(\boldsymbol{\xi}) = \varphi_\alpha(\boldsymbol{\xi})\mathbf{x}_\alpha \qquad \text{and} \qquad \mathbf{y}(\boldsymbol{\xi}) = \varphi_\alpha(\boldsymbol{\xi})\mathbf{y}_\alpha, \tag{7}$$

in which $\mathbf{x}_\alpha$ and $\mathbf{y}_\alpha$ denote respectively the initial and current position of each node α, and φ_α is the shape function associated with node α, defined on an auxiliary finite element with dimensionless coordinates $\boldsymbol{\xi}$, taken in this work as Lagrange polynomials. The elements used in this work are triangular with 3 nodes (linear interpolation) and 10 nodes (cubic interpolation)

By mapping the initial and current finite elements from this auxiliary one, we write

$$\mathbf{A} = \mathbf{A}^1 \left(\mathbf{A}^0\right)^{-1}, \tag{8}$$

where $\mathbf{A}^0$ and $\mathbf{A}^1$ are respectively the initial and current deformation gradient, calculated by the following expressions:

$$A^0_{ij} = \frac{\partial \varphi_\alpha}{\partial \xi_j} x^\alpha_i \qquad \text{and} \qquad A^1_{ij} = \frac{\partial \varphi_\alpha}{\partial \xi_j} y^\alpha_i. \tag{9}$$

Therefore, one can write the Green-Lagrange strain tensor entirely in terms of the initial and current nodal positions, and, consequently, calculate the second Piola-Kirchhoff tensor, given by

$$\mathbf{S} = \frac{\partial \Psi}{\partial \mathbf{E}}, \tag{10}$$

where Ψ is the Helmholtz free energy, defined by the constitutive model.

The solid mechanics problem consists of solving, for each node α, the equilibrium equation

$$\mathbf{f}^\alpha_{int} + \mathbf{f}^\alpha_{ext} = \mathbf{0}, \tag{11}$$

where $\mathbf{f}^\alpha_{ext}$ is the external force vector of α, and $\mathbf{f}^\alpha_{int}$ is the internal forces vector, written as

$$\mathbf{f}^\alpha_{int} = \int_{V_0} \mathbf{S} : \frac{\partial \mathbf{E}}{\partial \mathbf{y}^\alpha} \, dV_0. \tag{12}$$

Therefore, the equilibrium equations form a non-linear system can be written entirely in terms of the nodal positions, which is solved iteratively by Newton-Raphson method.

4 Constitutive model

4.1 Energy, stress and dissipation

Based on rheological models, we decompose the Helmholtz free energy (Ψ) additively by an elastic (Ψ_e), a visco-plastic isotropic (Ψ^{iso}_{vp}) and a visco-plastic kinematic (Ψ^{kin}_{vp}) part, where the first depends

only on the elastic strain, the second, only on the visco-plastic elastic strain, and the third, only on the hardening parameter (κ), i.e.:

$$\Psi(\mathbf{E}_e, \mathbf{E}^e_{vp}, \kappa) = \Psi_e(\mathbf{E}_e) + \Psi^{kin}_{vp}(\mathbf{E}^e_{vp}) + \Psi^{iso}_{vp}(\kappa). \tag{13}$$

Following, we define the elastic stress, the back stress tensor at initial configuration and the yield stress, respectively, as

$$\mathbf{S_e} = \frac{\partial \Psi_e}{\partial \mathbf{E}_e}, \qquad \mathbf{X} = \frac{\partial \Psi^{kin}_{vp}}{\partial \mathbf{E}^e_{vp}} \qquad \text{and} \qquad \sigma_\kappa = \frac{\partial \Psi^{iso}_{vp}}{\partial \kappa}, \tag{14}$$

where, in this work, Ψ_e and Ψ^{kin}_{vp} are assumed to be in the following neo-Hookean form:

$$\Psi^e = \frac{\Lambda}{2}\ln(J_e)^2 + \mu[\text{tr}(\mathbf{E}_e) - \ln(J_e)] \qquad \text{and} \qquad \Psi^{kin}_{vp} = \frac{c}{2}\text{tr}(\mathbf{E}^e_{vp}), \tag{15}$$

with tr$(\cdot)$ denoting the trace of a tensor, Λ and μ being the Lamé constants, and c the kinematic hardening stiffness. For the yield stress, the following linear rule is applied:

$$\sigma_\kappa(\kappa) = \sigma_Y + E_t\kappa. \tag{16}$$

where σ_Y is the initial yield stress, and E_t is the visco-plastic modulus.

The internal dissipation rate is given by the second law of thermodynamics, in the form of the Clausius-Duhem inequality:

$$d_{int} = \mathbf{S} : \dot{\mathbf{E}} - \dot{\Psi} \geq 0. \tag{17}$$

Finally, by applying the Coleman-Noll procedure (Coleman and Noll [23]) on Eq. (17), one can obtain the following expression for the second Piola-Kirchhoff stress tensor:

$$\mathbf{S} = \mathbf{A}^{-1}_{vp}\mathbf{S}_e\mathbf{A}^{-T}_{vp}. \tag{18}$$

4.2 Yield criterion and evolution laws

In this work, the von Mises yield criterion is adopted, as it is one of the most representative and widely applied criteria for ductile materials. It can be written as:

$$\Phi(\mathbf{M}_e, \boldsymbol{\chi}, \sigma_\kappa) = \|(\mathbf{M}_e - \boldsymbol{\chi})^D\| - \sqrt{\frac{2}{3}}\sigma_\kappa \leq 0, \tag{19}$$

where $(\cdot)^D$ denotes the deviatoric part of a tensor, $\mathbf{M}_e = \mathbf{A}^T_e\mathbf{A}_e\mathbf{S}_e$ is the Mandel tensor, and $\boldsymbol{\chi} = \mathbf{A}^e_{vp}\mathbf{X}(\mathbf{A}^e_{vp})^T$ is the back stress tensor at the intermediate configuration. More details on this criterion can be seen, for instance, in Dettmer and Reese [6].

The evolution of the visco-plastic deformation is given by the Perzyna model, which is obtained here by maximization of Eq. (17) (principle of maximum dissipation) restricted via penalty method to the yield criterion. The resulting equation is:

$$\dot{\mathbf{A}}_{vp} = \frac{\langle \Theta \rangle}{\eta} \mathbf{N} \mathbf{A}_{vp}, \tag{20}$$

where η is the viscosity parameter, $\mathbf{N}$ is a tensor that defines the direction of the evolution, Θ is the so-called overstress function, and $\langle \cdot \rangle$ denotes the Macauley brackets:

$$\langle \Theta \rangle = \frac{1}{2}(\Theta + |\Theta|). \tag{21}$$

In associative flow rules, $\mathbf{N}$ is assumed to be orthogonal to the yield surface. Therefore, it can be calculated by:

$$\mathbf{N} = \frac{\partial \Phi}{\partial \mathbf{M}_e} = \frac{(\mathbf{M}_e - \boldsymbol{\chi})^D}{\|(\mathbf{M}_e - \boldsymbol{\chi})^D\|}. \tag{22}$$

For the overstress function, as in Heeres et al. [11], we apply the Norton's law, given by:

$$\Theta = \left(\frac{\Phi}{\alpha} \right)^m, \tag{23}$$

being α and m calibration parameters. According to Heeres et al. [11], the condition $m \geq 1$ must be satisfied in order to achieve the necessary convexity of the overstress function.

The kinematic hardening is given by a finite strain generalization of the Armstrong-Frederick model, as shown in the works of Vladimirov et al. [16] and Brepols et al. [17]. The evolution law is written in terms of the $\mathbf{A}^i_{vp}$ tensor, by the expression:

$$\dot{\mathbf{A}}^i_{vp} = \frac{\langle \Theta \rangle}{\eta} \frac{b}{c} (\mathbf{M}^e_{vp})^D \mathbf{A}^i_{vp}, \tag{24}$$

where $\mathbf{M}^e_{vp} = (\mathbf{A}^e_{vp})^T \mathbf{A}^e_{vp} \mathbf{X}$ is a Mandel-like tensor, and b is a dimensionless parameter.

Lastly, for the isotropic hardening the following evolution law is applied:

$$\dot{\kappa} = \frac{\langle \Theta \rangle}{\eta} \sqrt{\frac{2}{3}}, \tag{25}$$

For the computational implementation, we apply the implicit Euler algorithm to perform the time integration of Eqs. (20), (24) and (25), which gives

$$\begin{cases} \dot{\mathbf{A}}_{vp} \approx \dfrac{\mathbf{A}^s_{vp} - \mathbf{A}^{s-1}_{vp}}{\Delta t} = \left(\dfrac{\langle \Theta \rangle}{\eta} \mathbf{N} \mathbf{A}_{vp} \right)^s, \\ \dot{\mathbf{A}}^i_{vp} \approx \dfrac{(\mathbf{A}^i_{vp})^s - (\mathbf{A}^i_{vp})^{s-1}}{\Delta t} = \left(\dfrac{\langle \Theta \rangle}{\eta} \dfrac{b}{c} (\mathbf{M}^e_{vp})^D \mathbf{A}^i_{vp} \right)^s, \\ \dot{\kappa} \approx \dfrac{\kappa^s - \kappa^{s-1}}{\Delta t} = \dfrac{\langle \Theta \rangle^s}{\eta} \sqrt{\dfrac{2}{3}}, \end{cases} \tag{26}$$

where the indexes $(\cdot)^s$ and $(\cdot)^{s-1}$ indicate variables from the current and previous time step, respectively. The system of equations (26) is non-linear, being solved, in this work, by the Newton-Raphson method, from which the plastic variables of the current step, $\mathbf{A}_{vp}^s$, $(\mathbf{A}_{vp}^i)^s$ and κ^s, are calculated.

5 Numerical examples

In this section we present numerical examples to show some characteristics of the proposed elasto-visco-plastic model, such as its response to different strain rates. The computational code is built in Fortran language, together with OpenMP for multi-threading. To solve the linear systems in the iterative processes, we use the HSL MA67 library (HSL [24]). For mesh generation and post-processing visualization, we make use of the Open-Source applications Gmsh (Geuzaine and Remacle [25]) and Paraview (Ayachit [26]), respectively.

5.1 Simple shear at small strain

This example, proposed originally by Heeres et al. [11], is presented in this work with the aim of showing the equivalence of the presented model with classical small strain Perzyna-type models. It consists of a cube with dimensions 1m x 1m x 1m, with restrictions and prescribed displacements applied as shown in Fig. 2: Dirichlet conditions in the lower and upper boundaries, and Neumann conditions with null forces in the left and right boundaries. Two cases are considered for the evolution of the prescribed displacements: loading-unloading (case I) and progressive deformation (case II), both with plane strain state.

Since the aim of this example is to obtain the stress-strain diagram for a single point with constant strain rate, a refined mesh is not needed. Therefore, we consider a mesh consisting of 2 triangular elements of linear order, with 1 integration point each, where the stress-strain diagram is measured (being equal for both elements).

The time discretization is as such: for the case I, 60 load steps are considered, with time increment of $\Delta t = 1.77 \cdot 10^{-5}$s each; for the case II, 40 load steps are considered, with time increment of $\Delta t = 4.35 \cdot 10^{-5}$s each.

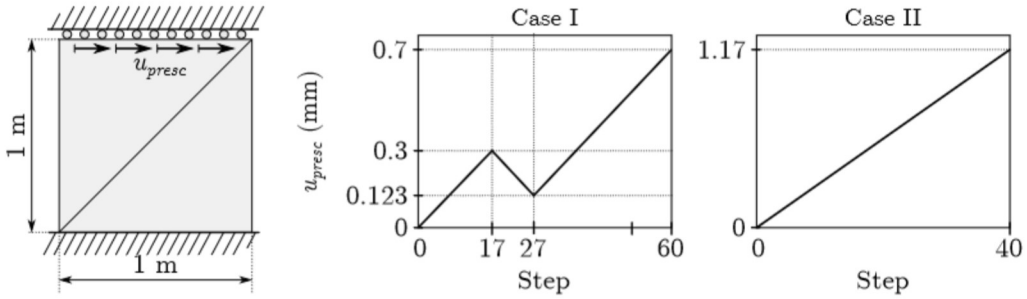

Figure 2. Geometry and load evolution for the small strain simple shear example

The hardening model is assumed to be only linear isotropic (no kinematic hardening). Since in the work of Heeres et al. [11] a different form of the von Mises yield criterion is adopted, a calibration of the visco-plastic parameters is performed in order to achieve the desired results. The calibrated parameters are given in Table 1.

The stress-strain response for both loading cases are given in Fig. 3, where a good agreement can be seen with the results of Heeres et al. [11]. The linear shear strain is given by u_{presc}/h, where h is the height of the cube (1 m), and the Cauchy stress tensor can be calculated by the equation

$$\boldsymbol{\sigma} = \frac{1}{J}\mathbf{A}\mathbf{S}\mathbf{A}^T, \tag{27}$$

Table 1. Material parameters for the small strain simple shear examples

E (Pa)	ν (Pa)	σ_Y (Pa)	E_t (Pa)	η (s)	α (Pa)	m
$2 \cdot 10^7$	0.2	$2 \cdot 10^3$	$-5 \cdot 10^6$	$2/3$	$2 \cdot 10^3$	1

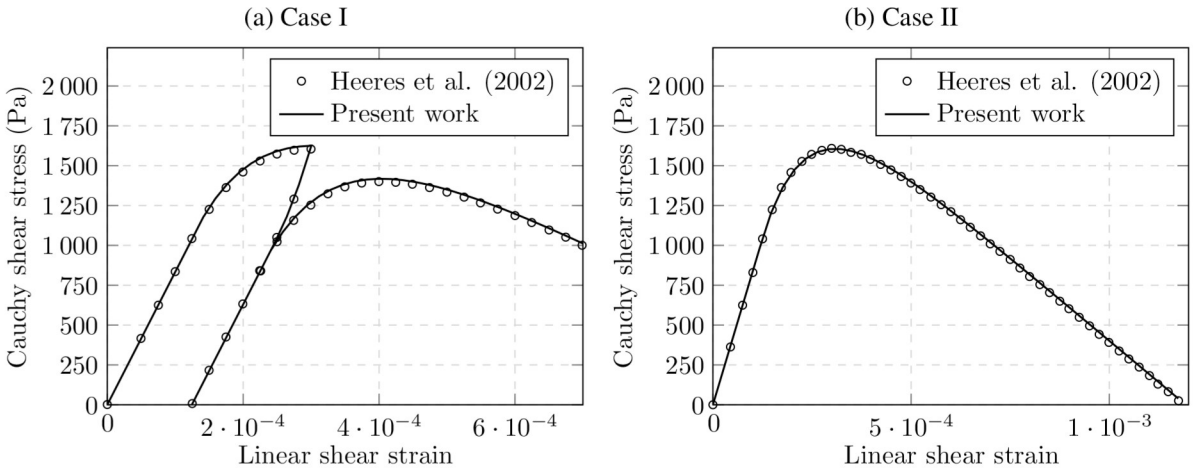

Figure 3. Stress-strain diagrams for the small strain simple shear example

5.2 Uniaxial tension and simple shear at large strain

This example is presented to show the stress-strain behavior of the model when subject to different strain rates. Again, we consider a cube with dimensions 1m x 1m x 1m, subject this time to large strain uniaxial tension and simple shear. For the uniaxial tension, the geometry and loads are shown in Fig. 4, with Dirichlet conditions at the left and lower boundaries, Neumann condition at the right and upper boundaries, and plane stress state; for the simple shear, the geometry and loads are shown in Fig. 5, with boundary conditions analogous to the example of section 5.1, and plane strain state.

The adopted mesh is the same from the previous example, and, again, two cases are considered for the evolution of the prescribed displacements: loading-unloading (case I), and progressive loading with fixed displacement at the final stage (case II). The last case represents a relaxation test and is performed to show the evolution of the yield stress at fixed strain. A total of 1200 steps is considered for both cases, being the maximum time (t_f) variable.

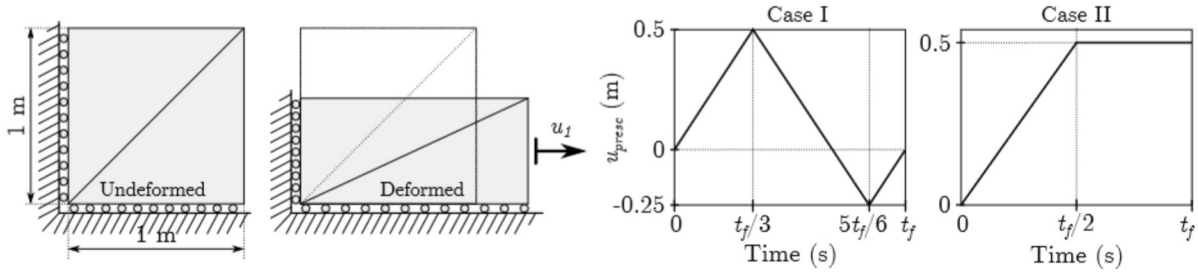

Figure 4. Geometry and load evolution for the large strain uniaxial tension example

The adopted material is the Mild Steel Ck-15, whose parameters are originally given by Lührs et al. [27] and calibrated for the presented model. This time, kinematic hardening is considered instead of isotropic, which means that the yield stress does not depend on the variable κ. The calibrated parameters are given in Table 2.

For the case I, the stress-strain diagrams are shown in Fig. 6 for different strain rates, together with

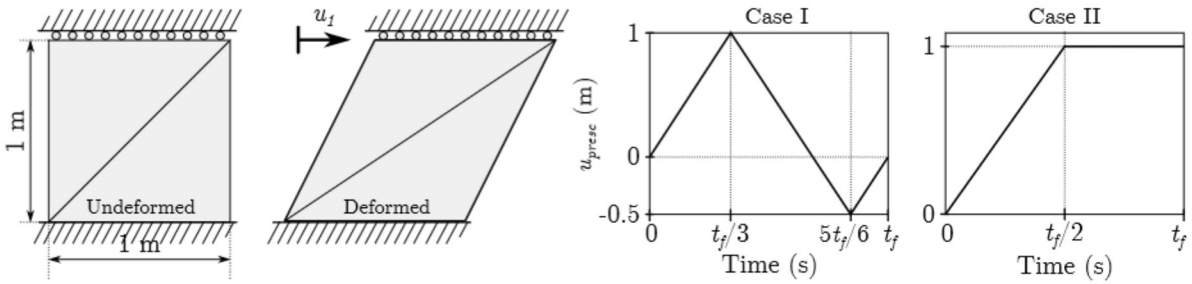

Figure 5. Geometry and load evolution for the large strain simple shear example

Table 2. Material parameters for the uniaxial tension and simple shear examples

Λ (MPa)	μ (MPa)	σ_Y (MPa)	E_t (MPa)	c (MPa)	b	η (s)	α (MPa)	m
173 333	80 000	300	0	1 900	8.5	$4 \cdot 10^4$	1	4

the equivalent elasto-plastic response, given by Dettmer and Reese [6]. As can be seen, the yield stress increases for higher strain rates (i.e., lower values of t_f), which consequently increases the general stress response. Furthermore, an interesting aspect of the Perzyna model can be noticed: for lower strain rates (i.e., higher values of t_f), the response approaches the elasto-plastic one. In other words, the elasto-plastic model of Dettmer and Reese [6] is equivalent to the proposed elasto-visco-plastic model at an infinitely slow rate, showing indeed that the latter can be treated as a generalization of the first.

For the case II, we show in Fig. 7 the time evolution of the Cauchy stress. In the progressive prescribed displacement stage, one can notice a similar response to the case I, i.e., higher stress responses for lower values of t_f. However, the interesting result lies in the second stage: as the strain is kept fixed, the stress values decrease and tend to the elasto-plastic response as the time evolves, which is a well known characteristic of the Perzyna model.

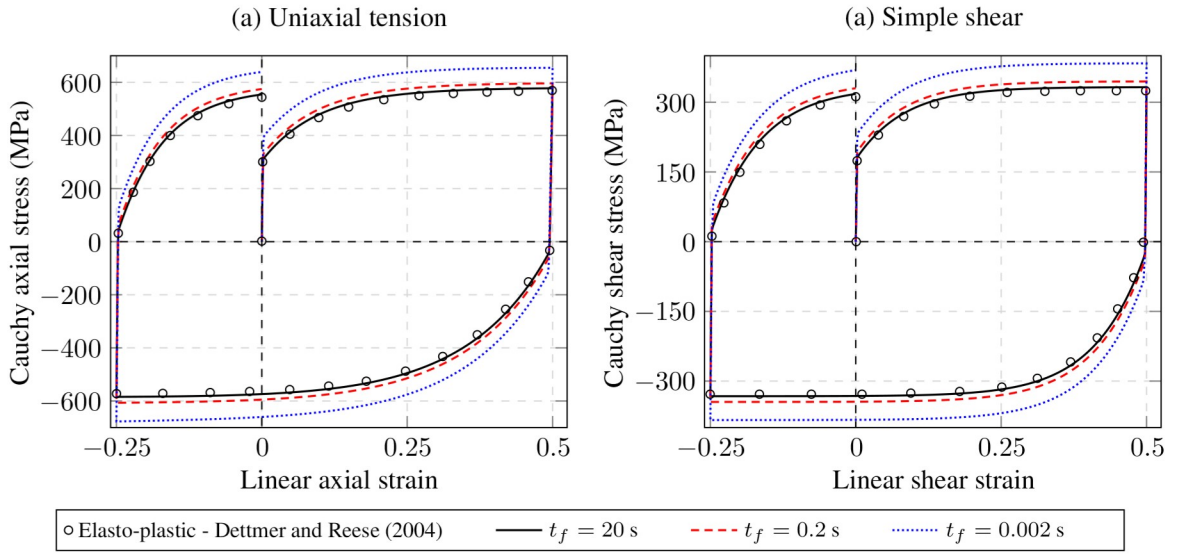

Figure 6. Stress-strain diagrams for the loading-unloading case

5.3 Partially loaded block

This example consists of a block with geometry and loads given by Fig. 8, and plane strain state. Taking advantage of the symmetry, only half of the problem is discretized, being adopted a regular

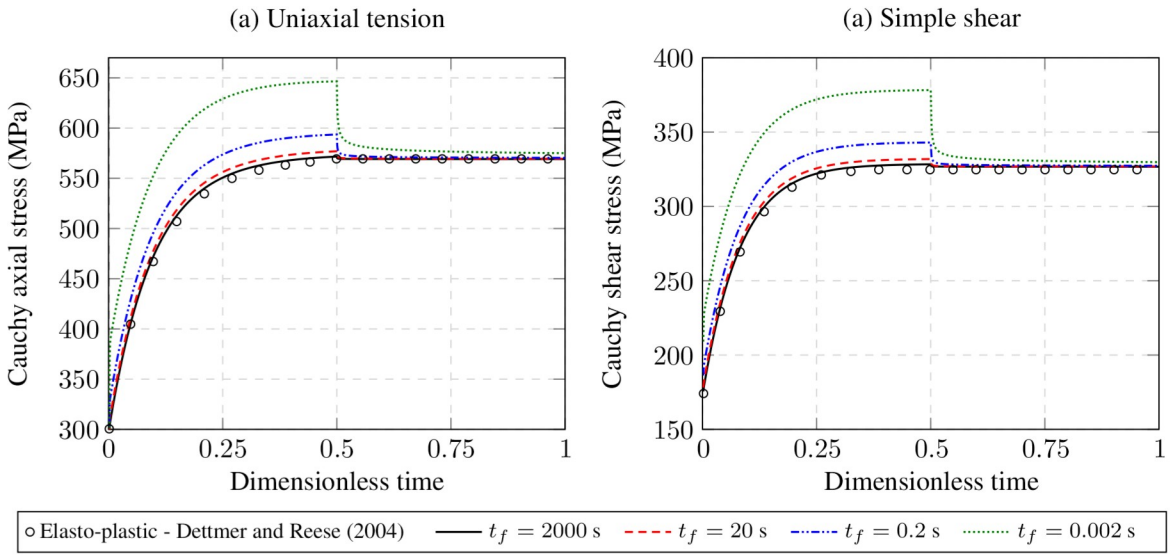

Figure 7. Stress evolution for the relaxation test case

mesh with 200 triangular elements of cubic approximation and 961 nodes. A total of 4000 time steps is adopted, being 2000 for the loading and 2000 for the unloading, with the maximum time (t_f) variable.

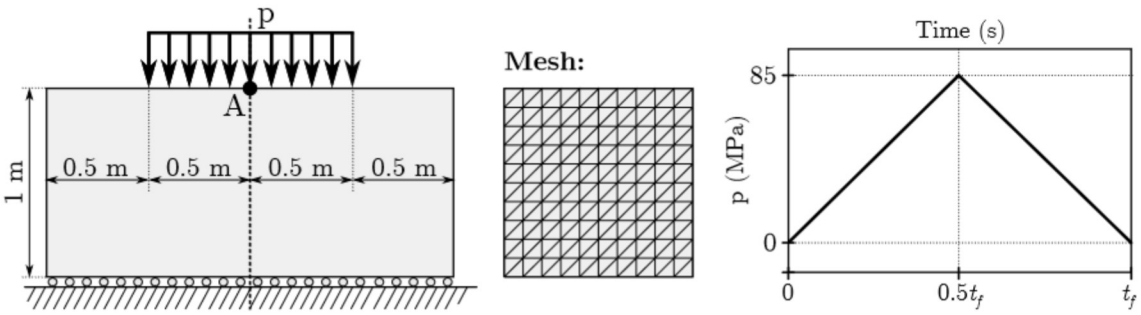

Figure 8. Geometry and mesh for the partially loaded block example

The material is assumed to be polymeric, with parameters given on Table 3, which are based on the oriented PET material presented in Lührs et al. [27]. Again, only kinematic hardening is considered.

Table 3. Material parameters for the partially loaded block example

Λ (MPa)	μ (MPa)	σ_Y (MPa)	E_t (MPa)	c (MPa)	b	η (s)	α (MPa)	m
320	80	35	0	100	2.7	1	35	1

The force-displacement diagram is shown in Fig. 9 for different values of t_f. In this example we can observe that the displacements values increases as the load rate decreases (i.e., as the value of t_f increases), since it approaches an elasto-plastic behaviour. Furthermore, as the load rate increases, the hysteresis effect of the loading-unloading curve decreases and the residual displacement tends to zero, suggesting that the results approaches a pure hyperelastic one. This is due to the excessive increase of the yield stress induced by the Perzyna model for higher rates.

In the Fig. 10, we show the deformed configurations for the totally loaded and the unloaded step in some of the cases analyzed.

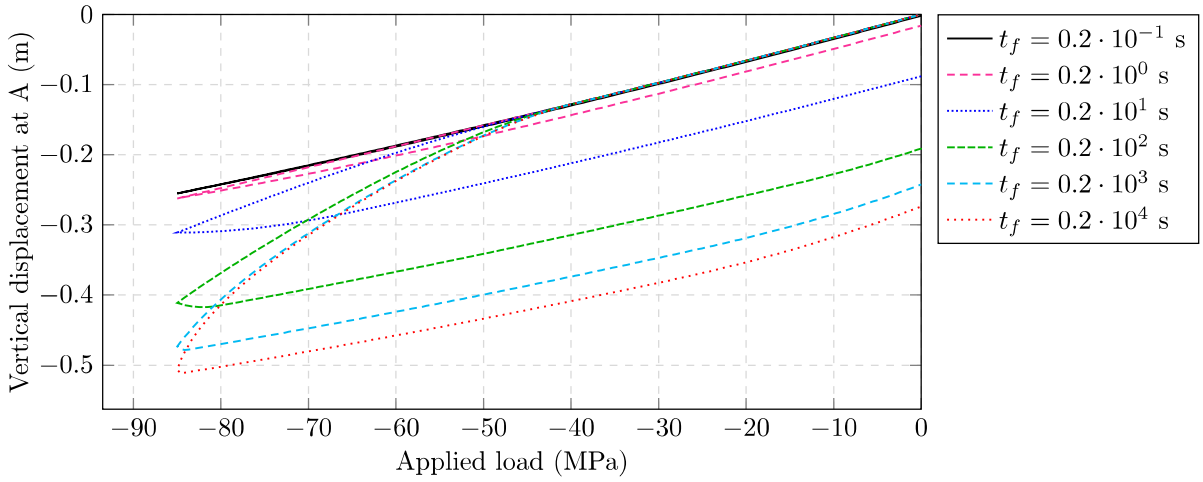

Figure 9. Force-displacement diagram for the partially loaded example

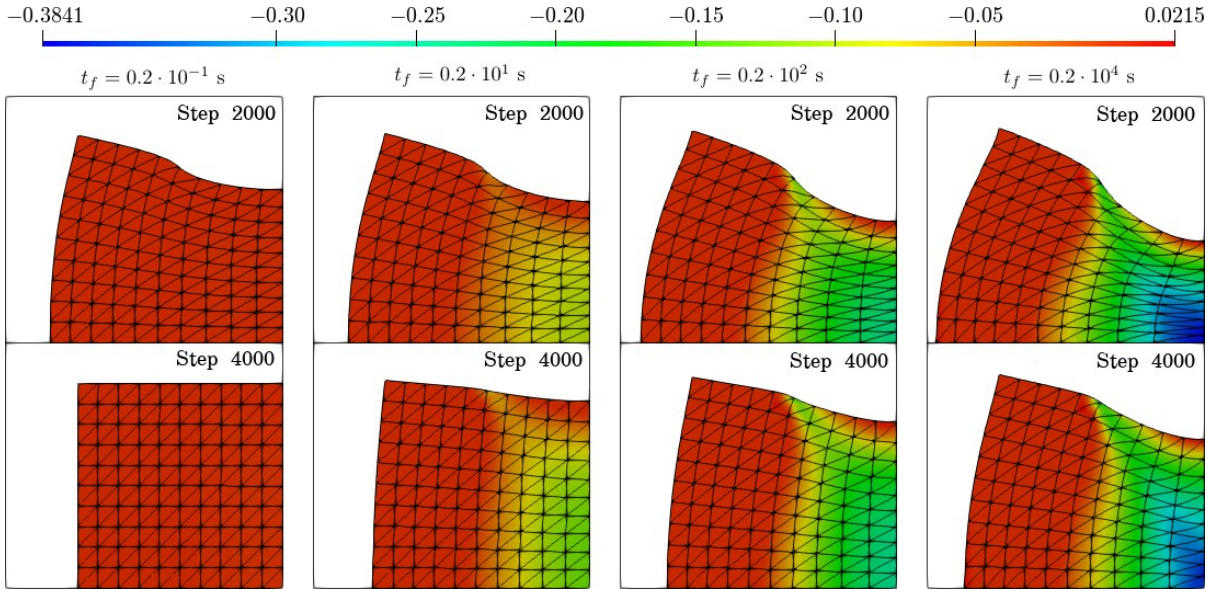

Figure 10. Deformed configurations of the partially loaded example, with component $(E_p)_{22}$ of plastic strain showed in color map

6 Conclusion

In this work we present and implement a numerical formulation for 2D modeling of large strain elasto-visco-plastic solids considering plane stress or plane stain, based on Perzyna model. Such formulation matches with the results of the classical small strain formulation, as can be see from the example in section 5.1. Another important characteristic of the model, is the association with the elasto-plastic response for infinitely small strain rates, as shown in the example from section 5.2. The relaxation test also behaves as expected from a Perzyna-like model, since the stress tends to the elasto-plastic yield stress as the time evolves. Furthermore, for larger strain rates, the results approach a pure hyperelastic one, as shown in section 5.3, which may not be representative for some specific materials. In such cases, a different elasto-visco-plastic model should be applied, or at least a modified version of the Perzyna model, as the one proposed by Mähler et al. [28].

Acknowledgements

The authors would like to acknowledge the Brazilian agency National Council for Scientific and Technological Development (CNPq), the *Coordenação de Aperfeiçoamento de Pessoal de Nível Superior* (CAPES) and the São Paulo Research Foundation (FAPESP) for the financial support given to this research.

Funding

This study was financed in part by the *Coordenação de Aperfeiçoamento de Pessoal de Nível Superior - Brasil* (CAPES) - finance code 001, by Brazilian National Council for Research and Technological Development (CNPq) - grant 310482/2016-0 and by São Paulo Research Foundation (FAPESP) - Process Number 2018/23957-2.

References

[1] Kröner, E., 1960. Allgemeine kontinuumstheorie der versetzungen und eigenspannungen. *Archive for Rational Mechanics and Analysis*, vol. 4, n. 4, pp. 273–334.

[2] Lee, E. H., 1969. Elastic-plastic deformation at finite strains. *Journal of Applied Mechanics*, vol. 36, n. 1, pp. 1–6.

[3] Haupt, P., 1985. On the concept of an intermediate configuration and its application to a representation of viscoelastic-plastic material behavior. *International Journal of Plasticity*, vol. 1, n. 4, pp. 303 – 316.

[4] Simo, J., 1985. On the computational significance of the intermediate configuration and hyperelastic stress relations in finite deformation elastoplasticity. *Mechanics of Materials*, vol. 4, n. 3, pp. 439 – 451.

[5] Svendsen, B., 1998. A thermodynamic formulation of finite-deformation elastoplasticity with hardening based on the concept of material isomorphism. *International Journal of Plasticity*, vol. 14, n. 6, pp. 473 – 488.

[6] Dettmer, W. & Reese, S., 2004. On the theoretical and numerical modelling of armstrong-frederick kinematic hardening in the finite strain regime. *Computer Methods in Applied Mechanics and Engineering*, vol. 193, n. 1, pp. 87 – 116.

[7] Pascon, J. & Coda, H., 2013a. Large deformation analysis of elastoplastic homogeneous materials via high order tetrahedral finite elements. *Finite Elements in Analysis and Design*, vol. 76, pp. 21 – 38.

[8] Perzyna, P., 1966. Fundamental problems in viscoplasticity. volume 9 of *Advances in Applied Mechanics*, pp. 243 – 377. Elsevier.

[9] Wang, W. M., Sluys, L. J., & de Borst, R., 1997. Viscoplasticity for instabilities due to strain softening and strain-rate softening. *International Journal for Numerical Methods in Engineering*, vol. 40, n. 20, pp. 3839–3864.

[10] Simo, J. & Hughes, T., 2000. *Computational Inelasticity*. Interdisciplinary Applied Mathematics. Springer New York.

[11] Heeres, O. M., Suiker, A. S., & de Borst, R., 2002. A comparison between the perzyna viscoplastic model and the consistency viscoplastic model. *European Journal of Mechanics - A/Solids*, vol. 21, n. 1, pp. 1 – 12.

[12] Ibrahimbegović, A. & Chorfi, L., 2000. Viscoplastic model at finite deformations with combined isotropic and kinematic hardening. *Computers & Structures - COMPUT STRUCT*, vol. 77, pp. 509–525.

[13] Ponthot, J., 2002. Unified stress update algorithms for the numerical simulation of large deformation elasto-plastic and elasto-viscoplastic processes. *International Journal of Plasticity*, vol. 18, n. 1, pp. 91 – 126.

[14] Garino, C. G., Vairo, M. R., Fagés, S. A., Mirasso, A., & Ponthot, J.-P., 2013. Numerical simulation of finite strain viscoplastic problems. *Journal of Computational and Applied Mathematics*, vol. 246, pp. 174 – 184. Fifth International Conference on Advanced COmputational Methods in ENgineering (ACOMEN 2011).

[15] Careglio, C., Canales, C., García Garino, C., Mirasso, A., & Ponthot, J. P., 2016. A numerical study of hypoelastic and hyperelastic large strain viscoplastic perzyna type models. *Acta Mechanica*, vol. 227, n. 11, pp. 3177–3190.

[16] Vladimirov, I. N., Pietryga, M. P., & Reese, S., 2010. Anisotropic finite elastoplasticity with nonlinear kinematic and isotropic hardening and application to sheet metal forming. *International Journal of Plasticity*, vol. 26, n. 5, pp. 659 – 687.

[17] Brepols, T., Vladimirov, I. N., & Reese, S., 2014. Numerical comparison of isotropic hypo- and hyperelastic-based plasticity models with application to industrial forming processes. *International Journal of Plasticity*, vol. 63, pp. 18 – 48. Deformation Tensors in Material Modeling in Honor of Prof. Otto T. Bruhns.

[18] Lion, A., 2000. Constitutive modelling in finite thermoviscoplasticity: a physical approach based on nonlinear rheological models. *International Journal of Plasticity*, vol. 16, n. 5, pp. 469 – 494.

[19] Coda, H. & Greco, M., 2004. A simple FEM formulation for large deflection 2D frame analysis based on position description. *Computer Methods in Applied Mechanics and Engineering*, vol. 193, n. 33, pp. 3541 – 3557.

[20] Coda, H. B., 2009. A solid-like FEM for geometrically non-linear 3D frames. *Computer Methods in Applied Mechanics and Engineering*, vol. 198, n. 47, pp. 3712 – 3722.

[21] Coda, H. B. & Paccola, R. R., 2010. Improved finite element for 3D laminate frame analysis including warping for any cross-section. *Applied Mathematical Modelling*, vol. 34, n. 4, pp. 1107 – 1137.

[22] Coda, H. B. & Paccola, R. R., 2014. A total-lagrangian position-based FEM applied to physical and geometrical nonlinear dynamics of plane frames including semi-rigid connections and progressive collapse. *Finite Elements in Analysis and Design*, vol. 91, pp. 1 – 15.

[23] Coleman, B. D. & Noll, W., 1963. The thermodynamics of elastic materials with heat conduction and viscosity. *Archive for Rational Mechanics and Analysis*, vol. 13, n. 1, pp. 167–178.

[24] HSL, 2013. A collection of fortran codes for large scale scientific computation. http://www.hsl.rl.ac.uk/.

[25] Geuzaine, C. & Remacle, J.-F., 2009. Gmsh: a three-dimensional finite element mesh generator with built-in pre- and post-processing facilities. *International Journal for Numerical Methods in Engineering*, vol. 79, pp. 1309 – 1331.

[26] Ayachit, U., 2015. *The ParaView Guide: A Parallel Visualization Application*. Kitware, Inc., USA.

[27] Lührs, G., Hartmann, S., & Haupt, P., 1997. On the numerical treatment of finite deformations in elastoviscoplasticity. *Computer Methods in Applied Mechanics and Engineering*, vol. 144, n. 1, pp. 1–21.

[28] Mähler, L., Ekh, M., & Runesson, K., 2001. A class of thermo-hyperelastic–viscoplastic models for porous materials: theory and numerics. *International Journal of Plasticity*, vol. 17, n. 7, pp. 943 – 969.